Quadrotor Safe Flight Envelope Prediction in the High-Speed Regime: A Monte-Carlo Approach

Sun, Sam; de Visser, Coen

DOI
10.2514/6.2019-0948

Publication date
2019

Document Version
Final published version

Published in
AIAA Scitech 2019 Forum

AIAA SciTech Forum
7-11 January 2019, San Diego, California
AIAA Scitech 2019 Forum

10.2514/6.2019-0948

Quadrotor Safe Flight Envelope Prediction in the High-Speed Regime: A Monte-Carlo Approach

S. Sun,* C.C. de Visser†

Delft University of Technology, 2629HS Delft, The Netherlands

The Safe Flight Envelope (SFE) is a prerequisite for flight envelope protection and essential for preventing Loss of Control (LoC) of a flying vehicle. Reachability analysis has been proposed for defining a SFE considering the dynamic characteristics of a system. However, the conventional Level Set approach for conducting reachability analysis is computational inefficient and impractical to solve problems having a state space with more than 4 dimensions. For this, we have proposed a computational efficient Monte-Carlo (MC) based approach. As an application, the SFE of an off-the-shelf quadrotor during the high-speed forward flight are estimated, based on the aerodynamic model identified from the high-speed flight data ($V < 16$ m/s). Taking into account the actuator dynamics, the state space of the problem has 6 dimensions in excess of the computational capabilities of the Level Set approach. By contrast, the result shows that the Monte-Carlo simulation based approach is able to solve this high dimension problem in a matter of seconds.

Nomenclature

V_x, V_z Velocity projection on the body frame, m/s
p, q roll rate and pitch rate, rad/s
V airspeed, m/s
θ pitch angle, rad
γ path angle, rad
α angle of attack, rad
Ω_1,Ω_2,Ω_3,Ω_4 rotor speeds, rad/s
h simulation time step, s
N segment number of the discretized trajectory
N_{traj} trajectory number of estimating a reachable set
p_s probability of changing the control input in the next simulation step
p_c probability of generating a trajectory with constant control inputs amongh N_{traj} trajectories
T time horizon of the reachable set, s
m mass of the quadrotor, kg
g gravitational acceleration, m/s^2
F_x,F_z resultant forces projecting on the body frame, N
M_y pitch moment projecting on the body frame, Nm
τ time constant of a first-order actuator dynamic model, s

I. Introduction

The safety of multi-rotor drones, such as quadrotor, has become a major concern because of the rapid growth of the drone industry. Loss of Control (LoC) is considered as a major factor of aviation accidents,

*Ph.D. student, Control and Simulation Division, Faculty of Aerospace Engineering, Kluyverweg 1, 2629HS Delft, The Netherlands; s.sun-4@tudelft.nl

†Assistant professor, Control and Simulation Division, Faculty of Aerospace Engineering, Kluyverweg 1, 2629HS Delft, The Netherlands. AIAA Member

which has contributed to more than 22 accidents of commercial aircraft in the fixed-wing configurations since 1999.[1] On the other hand, for the multi-rotor vehicles which is inherently unstable, preventing the LoC is a crucial factor of improving their safety and should be fully investigated.[2]

There is an extensive body of literature focus on the issue of Safe Flight Envelop Protection (SFEP). As a prerequisite, a Safe Flight Envelop (SFE) must be predicted within which the LoC can be effectively avoided. A quantitative approach of defining the LoC and five safe envelopes for commercial fixed-wing aircraft was proposed[3] and several following researches were carried out.[4–6] However, it is inappropriate to utilize these approaches to a quadrotor vehicle because of its distinction from the fixed-wing aircraft in terms of flight mechanism.

By contrast, the physical approach[7] based on the aerodynamic forces and moments model instead of the statistics is possible to be utilized to a quadrotor. In the physical approach, the reachability analysis is carried out to estimate the forward and backward reachable set from the trim set in a given time horizon. As is shown in Fig. 1, the intersection of the forward and backward reachable sets are regarded as the SFE within which the vehicle possesses the ability to leave, and then, return the trim condition in a finite time period, based on the knowledge of its physical model. To this end, a global model need to be established to predict the dynamic of the vehicle and take into account its nonlinearity. Among different types of numerical methods for reachability analysis, the level set method was applied in estimating the reachable set of a fixed-wing aircraft.[8–10]

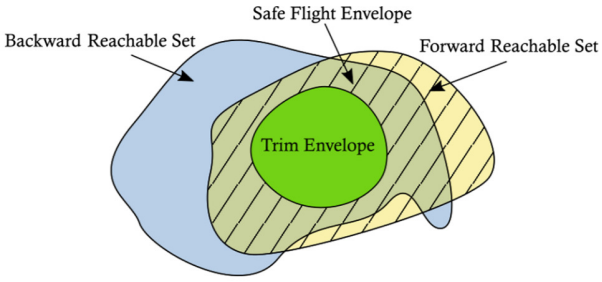

Figure 1: Forward backward reachable set and the definition of SFE.[9]

In comparison with the fixed-wing aircraft, the maneuverability of a multi-rotor vehicle is much greater. Therefore, the SFE should be defined in a much briefer time horizon in which the actuator dynamics of the quadrotor must be considered. As a consequence, additional states of the actuator need to be involved in the reachability analysis that the level set is unable to address due to the curse of dimensionality.[9,11] For this reason, alternative method must be employed.

Numerical simulation based method is another type of promising approach for reachability analysis,[12–14] especially for large dimensional problems.[15] For a nonlinear system, the reachable set is able to be estimated by performing infinite numbers of simulations with randomly sample the inputs, i.e. a random-walk Monte-Carlo Simulation approach. However, this can be time consuming.

In this research, a quadrotor is modeled as a nonlinear control-affine system that are linear in the input. Based on the viscosity solution of the Hamilton-Jacobi partial differential equation (HJB-PDE), a bang-bang control is proven optimal for a trajectory to reach the boundary of the reachable set, though the switching time still remains unknown. As a result, the search space of the system input is largely reduced and performing Monte-Carlo simulations becomes applicable to reachability analysis.

The quadrotor aerodynamic force and moment model in the high-speed flight regime, as well as the actuator model, are identified from the data of free flight tests conducted in the wind tunnel. Subsequently, the trim set are calculated from the aerodynamic models, and are regarded as the initial condition to estimate forward and backward reachable sets using the proposed Monte-Carlo approach. The method is found to be efficient since a reachable set with 6 dimensions can be estimated in a few seconds on a desktop computer.

This paper is organized as follows. Section II introduces the methodology. Section III presents the quadrotor longitudinal model and the trim condition. Section IV presents the result of Safe Flight Envelope, which is validated in the Section IV.B.

II. Methodology

II.A. Optimal Control for Reachability Analysis

Consider a nonlinear control-affine system

$$\dot{\boldsymbol{x}} = \boldsymbol{f}(\boldsymbol{x}, t) + \boldsymbol{g}(\boldsymbol{x}, t)\boldsymbol{u} \tag{1}$$

where $\boldsymbol{x} \in \mathcal{R}^n$, $\boldsymbol{u} \in \boldsymbol{U} = [\underline{\boldsymbol{u}},\ \bar{\boldsymbol{u}}]$. The definition of reachable set and invirant set can be characterized as[16]

$$\mathcal{R}(t, K) = \{\boldsymbol{x} \in \mathrm{R}^n | \exists \boldsymbol{u} \in \boldsymbol{U}, \exists \tau \in [t, T], \phi(\tau, t, \boldsymbol{x}, u(\cdot)) \in K\} \tag{2}$$

$$\mathcal{I}(t, K) = \{\boldsymbol{x} \in \mathrm{R}^n | \forall \boldsymbol{u} \in \boldsymbol{U}, \forall \tau \in [t, T], \phi(\tau, t, \boldsymbol{x}, u(\cdot)) \in K\} \tag{3}$$

where T is the time horizon, K is the target closed set, $\phi(\tau, t, \boldsymbol{x}, u(\cdot))$ is the state trajectory with $\boldsymbol{x}(t)$ as the initial state.

The principle of duality provides the relationship between the reachability and the invariance

$$\mathcal{R}(t, K) = (\mathcal{I}(t, K^c))^c \tag{4}$$

By calculating the invariant set, one can use the above relationship to determine the reachable set. Specifically, the reachable set $\mathcal{R}(t, K)$ and the invariant set $\mathcal{I}(t, K^c)$ share the same boundary, which is to be determined. The invariant set can be linked to an infiumum minimum optimal control problem

$$\mathcal{I}(t, K) = \left\{ \boldsymbol{x} \in \mathcal{R}^n | V_2(\boldsymbol{x}, t) = \inf_{\boldsymbol{u}(\cdot) \in \boldsymbol{U}_{[t,T]}} \min_{\tau \in [t,T]} l(\phi(\tau, t, \boldsymbol{x}, u(\cdot))) \geq 0) \right\} \tag{5}$$

where $K = \{\boldsymbol{x} \in \mathcal{R}^n | l(\boldsymbol{x}) \geq 0\}$ and $l(\boldsymbol{x})$ is a continuous function $l : \mathcal{R}^n \to \mathcal{R}$.

The viscosity solution of a Hamilton-Jacobi partial differential equation (HJB PDE) can be characterized as the solution of the value function V_2 in Eq. 5

$$\frac{\partial V_2}{\partial t}(\boldsymbol{x}, t) + \min \left\{ 0, \inf_{\boldsymbol{u}(\cdot) \in \boldsymbol{U}} \frac{\partial V_2}{\partial \boldsymbol{x}}(\boldsymbol{x}, t)(\boldsymbol{f}(\boldsymbol{x}, t) + \boldsymbol{g}(\boldsymbol{x}, t)\boldsymbol{u}) \right\} = 0 \tag{6}$$

The zero level set of the V_2 is the estimated boundary of the invariant set, and subsequently the boundary of the reachable set is obtained. The evolution of the boundary relies on the optimal control such that the infiumum term in Eq. 6 is realized

$$\boldsymbol{u}^\star(\boldsymbol{x}, t) = \operatorname*{argmin}_{\boldsymbol{u}(\cdot) \in \boldsymbol{U}_{[t,T]}} \frac{\partial V_2}{\partial \boldsymbol{x}}(\boldsymbol{x}, t)(\boldsymbol{f}(\boldsymbol{x}, t) + \boldsymbol{g}(\boldsymbol{x}, t)\boldsymbol{u}) \tag{7}$$

For notational simplicity, we define the array

$$\boldsymbol{\lambda}(\boldsymbol{x}, t) = \frac{\partial V_2}{\partial \boldsymbol{x}}(\boldsymbol{x}, t)\boldsymbol{g}(\boldsymbol{x}, t) \in \mathcal{R}^m \tag{8}$$

By virtue of the affine form of the system Eq. 1, the optimal control required in the HJB PDE can be chosen as

$$\boldsymbol{u}_i^\star(\boldsymbol{x}, t) = \begin{cases} \bar{\boldsymbol{u}}_i, & \boldsymbol{\lambda}_i(\boldsymbol{x}, t) < 0 \\ \underline{\boldsymbol{u}}_i, & \boldsymbol{\lambda}_i(\boldsymbol{x}, t) > 0 \end{cases} \tag{9}$$

Assume $\boldsymbol{\lambda}_i \neq 0$ almost everywhere, then the optimal control for calculating the reachable set lies on the boundary of the control constraint. This means that, trajectory initialized at the boundary of the reachable set is a solution of the bang-bang control. Therefore, while conducting a Monte-Carlo simulation, we can randomly sample the $\boldsymbol{u_i}(t)$ among $\{\underline{\boldsymbol{u}}_{\boldsymbol{i}},\ \bar{\boldsymbol{u}}_{\boldsymbol{i}}\}$ instead of the entire control space, and the sampling space of conducting a Monte-Carlo simulation can be significantly reduced.

II.B. Monte-Carlo Simulation

Given a time horizon T of the simulation, the trajectory can be discretized into N segments such that the time step equals $h = T/N$. Numerical methods for solving ordinary differential equations (ODE) such as 4th order Runge-Kutta method can be applied to iteratively calculate the predicted trajectory from an initial state $\boldsymbol{x}_0$ with given input $\boldsymbol{u}(\tau)_{\tau\in[k,k+h]}$ where $k = 0, 1, 2, ..., N-1$.

For brutal force simulation, the $\boldsymbol{u}(\cdot)$ is randomly sampled among $\boldsymbol{U}$ in every time step and lead to enormous number of possible trajectories to be simulated. With the aim of finding the boundary of reachable set, only $\boldsymbol{u}^\star$ as given in Eq. 9 need to be selected in each time step leading to a bang-bang control driven trajectory. To further decrease the number of required trajectory, a tuning parameter is defined to determine the probability of changing the control input from one extreme value to the other

$$p_s = 1 - P(u_i(k+h) = u_i(k)) \tag{10}$$

The selection of p_s is a major concern to guarantee that the trajectories are mostly ended at the boundary of the reachable set. A parameter denoted by p_c is designed to indicate the probability of a trajectory with constant control input

$$(1 - p_s)^N = p_c \tag{11}$$

The safe flight envelope is defined as the intersection of forward and backward reachable sets.[8,9] Therefore, the trajectories from Monte-Carlo Simulation for estimating the forward reachable set are initialized at the trim condition. Then the boundary of the forward reachable set can be approximated by the outer contour formed by the end points of these trajectories. As for the backward reachable set, the system equation (Eq. 1) is multiplied by -1 such that

$$\dot{\boldsymbol{x}} = -\boldsymbol{f}(\boldsymbol{x}, t) - \boldsymbol{g}(\boldsymbol{x}, \boldsymbol{t})\boldsymbol{u} \tag{12}$$

and the simulation is initialized at the target state (trimming) and backward propagate through time and end up at the initial state. In the following, we will employ this method to a quadrotor to compute the longitudinal safe flight envelope.

III. Problem Formulation

III.A. Modeling of Quadrotor Longitudinal Motions

The longitudinal model of quadrotor considering aerodynamic effect is given in this section. This model is used for estimating the trim curve, from which the backwards and forwards reachable sets is computed using the same model. For simplicity, only longitudinal dynamic is considered

$$\dot{V}_x = F_x/m - g\sin(\theta) - qV_z \tag{13}$$

$$\dot{V}_z = F_z/m + g\cos(\theta) + qV_x \tag{14}$$

$$\dot{\theta} = q \tag{15}$$

$$\dot{q} = M_y/I_y \tag{16}$$

where m and I_y stand for the mass and inertia of a quadrotor respectively; $\boldsymbol{x} = [V_x\ V_z\ \theta\ q]^T$ is longitudinal quadrotor state, namely the air-velocity component on the x_B and z_B axis, pitch angle and pitch rate. F_x, F_z and M_y are resultant forces (except the gravity) and moments. The tested quadrotor is a Parrot Bebop2 as Fig. 2 shows, together with the numbering of rotor speeds and the definition of the body frame with the origin at the center of mass.

The aerodynamic effects have been found to significantly affect the external forces and moments.[17,18] Therefore, a gray-box model of F_x, F_z and M_y is established from flight test data in the form of

$$F_x = C_{d,1}V_x + C_{d,2}V_x^2 + C_{d,3}V_x^3 + C_{d,4}V_z \tag{17}$$

$$F_z = C_{z,0(V_x,V_z)} + C_{z,1(V_x,V_z)}u_1 + C_{z,2(V_x,V_z)}u_2 \tag{18}$$

$$M_y = C_{m,0(V_x,V_z)} + C_{m,1(V_x,V_z)}u_1 + C_{m,2(V_x,V_z)}u_2 \tag{19}$$

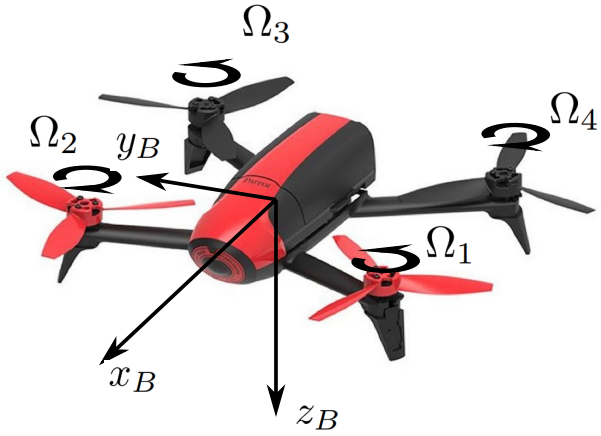

Figure 2: Tested quadrotor (Bebop2) and the numbering of rotor.

where $C_{\star(\cdot)}$ denotes a coefficient which depends on the variables in the bracket. u_1 and u_2 are the sum of square of front rotors and back rotors respectively.

$$[u_1,\ u_2] = [\Omega_1^2 + \Omega_2^2,\ \Omega_3^2 + \Omega_4^2] = [2\Omega_f^2, 2\Omega_b^2] \tag{20}$$

Due to the high maneuverability of a quadrotor, the time horizon of the reachability analysis can be very short. For this reason, the actuator dynamics become non-negligible. For simplicity, the actuator is modeled as a first-order system mapping from the command rotor speed to a real rotor speed.

$$\dot{u}_1 = -\tau u_1 + \tau u_{1,ref} \tag{21}$$

$$\dot{u}_2 = -\tau u_2 + \tau u_{2,ref} \tag{22}$$

The augmented problem, consequently, has 6 degrees of freedom.

The aerodynamic coefficients and the actuator dynamic model can be identified from the flight test data obtained in the wind tunnel. The model structure of F_x is determined while the structure of the other two models are selected using a stepwise regression method.[18,19] The estimated model structure and corresponding parameters in Eq. 17-19 are listed as follows:

$$\begin{aligned}
&C_{d,1} = -2.17 \times 10^{-1} \\
&C_{d,2} = 1.84 \times 10^{-2} \\
&C_{d,3} = -9.61 \times 10^{-4} \\
&C_{d,4} = 6.170460 \times 10^{-2} \\
&C_{z,0} = 2.98 \times 10^{-2}|V_z|V_z - 3.77 \times 10^{-3}V_z^3 \\
&C_{z,1} = 1.67 - 8.58 \times 10^{-2}V_x + 2.20 \times 10^{-3}V_x^2 \\
&C_{z,2} = 2.15 + 1.97 \times 10^{-2}V_x^2 + 7.28 \times 10^{-2}V_z - 6.84 \times 10^{-4}V_x^3 - 1.97 \times 10^{-4}V_x^3V_z + 4.34 \times 10^{-3}V_x^2V_z \\
&C_{m,0} = 1.03 \times 10^{-2}V_x - 6.77 \times 10^{-4}V_x^2 + 8.64 \times 10^{-3}V_z + 7.17 \times 10^{-5}V_x^2V_z + 2.63 \times 10^{-4}V_xV_z^2 \\
&C_{m,1} = 1.52 \times 10^{-1} + 1.04 \times 10^{-3}V_x^2 + 1.66 \times 10^{-3}V_xV_z - 1.86 \times 10^{-3}V_x \\
&C_{m,2} = -1.63 \times 10^{-1} + 8.04 \times 10^{-3}V_x - 2.11 \times 10^{-4}V_xV_z - 6.31 \times 10^{-4}V_x^2;
\end{aligned} \tag{23}$$

Fig. 3 provides the residual auto-correlation of the longitudinal force and moment model. The auto-correlations are mostly lying in the $2-\sigma$ confidence interval, showing an acceptable quality of the identified model.

III.B. Trim Condition

Similar to helicopters and fixed-wing aircrafts, a quadrotor vehicle also has a trim curve. Here we define the longitudinal trim as a condition such that the drone maintains level flight with constant flight speed and pitch angle. Therefore, states of the quadrotor should satisfy that

$$\gamma = \theta - \alpha = 0 \tag{24}$$

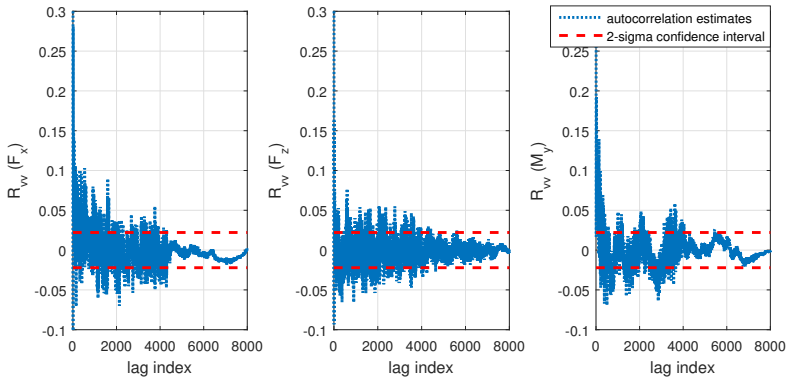

Figure 3: Residual autocorrelation of the F_x, F_z and M_y model.

where γ indicates the path angle, and $\alpha = \arctan(V_z/V_x)$ denotes the angle of attack of a quadrotor. To maintain the constant flight speed and pitch angle and by recalling Eq. 13-16, the following conditions need to be satisfied

$$\begin{aligned} F_x - mg\sin(\theta) &= 0 \\ F_z + mg\cos(\theta) &= 0 \\ M_y &= 0 \end{aligned} \tag{25}$$

Note that F_x, F_z and M_y are modeled as functions of u_1, u_2, V_x and V_y. Hence in different flight speed, the corresponding θ, u_1 and u_2 are able to be obtained by solving Eq. 25. The calculated trim curves based on the aerodynamic model Eq. 17-19 are illustrated in Fig. 4.

To validate the accuracy of the trim curve, the flight data selected in the following intervals are also plotted

$$\dot{V} \in [-0.5,\ 0.5]\mathrm{m/s}^2, \quad q \in [-5,\ 5]^\circ, \quad \dot{q} \in [-5,\ 5]^\circ/\mathrm{s}^2, \quad \gamma \in [-1,\ 1]^\circ \tag{26}$$

The θ-V curve accords with the observation that the faster the drone flights, the more negative pitch angle it should maintain. The Ω-V curve shows that larger rotor speeds are required for back rotors than front rotors according with the hypothesis that a nose-up moment is generated in the forward flight.[20] As the back rotors saturate, the drone reaches its highest level flight speed. This trim curve also indicates that the maximum flight speed of a quadrotor can be achieved by solely increasing the capacity of rear motors instead of all actuators.

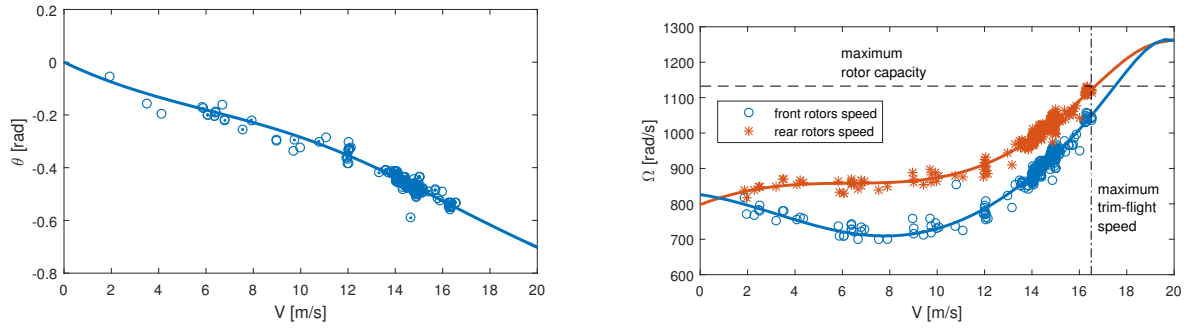

(a) Relationship of θ and V in the trim condition, compared with the flight data.

(b) The front and back rotors speed in the trim condition compared with the flight data.

Figure 4: Trim curve of the Bebop2 quadrotor in forward flight.

IV. Results

IV.A. Estimation of the Reachable Sets

The forward reachable set from the trim point at $V = 8$ m/s, $\theta = -13.1°$, $\Omega_f = 709.5$ rad/s and $\Omega_b = 860.4$ rad/s are computed for demonstration. The time horizon is chosen as $T = 0.15$ s, which is much more brief than those of a fixed-wing aircraft (at the magnitude of 1s) as the quadrotors have more agility than a fixed-wing. The trajectory is discretized into $N = 100$ segments and $N_{traj} = 1000$ trajectories are generated. The CPU of the computer performing the simulation is Intel(R) Xeon(R) E51620 v3 at 3.50GHz, the RAM is 16.0GB. As a result, a reachable set in a 6 dimension state space can be generated within 3.6 seconds.

In Fig. 5 and Fig. 6 the forward reachable sets are estimated with different p_c. It is evident that different selection of the control inputs are essential for the reachable set estimation. In this problem, a larger p_c indicates a larger probability of performing aggressive maneuvers that is essential for reaching the boundary of the reachable set. By contrast, the endpoints of MC simulations with smaller p_c mostly fall in the internal of the reachable set. This makes the reachable set estimated with a larger p_c less conservative comparing with a smaller p_c.

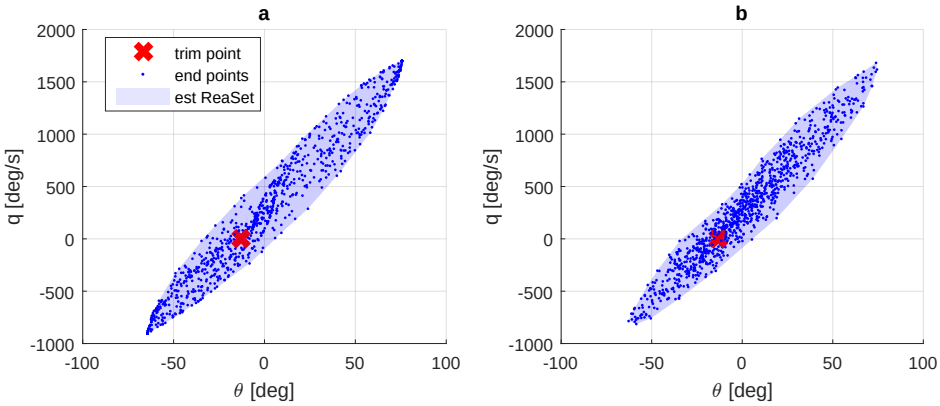

Figure 5: Forward reachable set projection on $q - \theta$ plane. a.) $p_c = 0.1$. b.) $p_c = 0.001$.

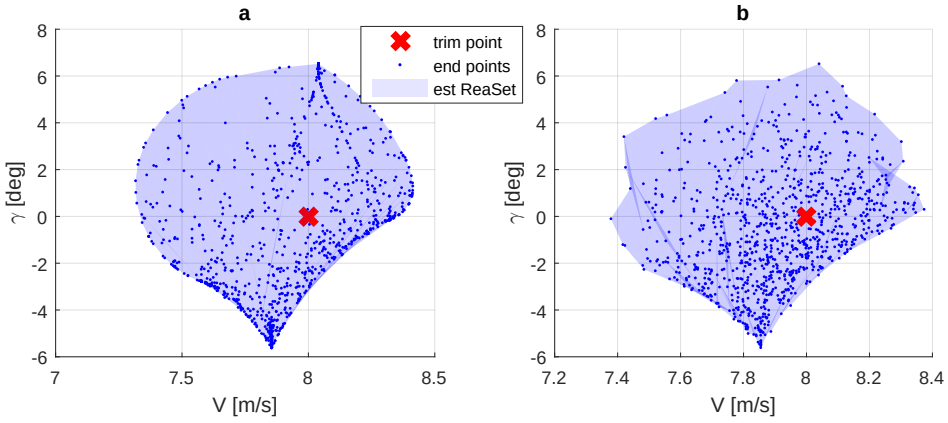

Figure 6: Forward reachable set projection on $V - \gamma$ plane. a.) $p_c = 0.1$. b.) $p_c = 0.001$.

The effect of actuator dynamics is demonstrated in Fig. 7. The reachable sets without actuator rate limits taken into account are much larger than those with actuators dynamics. This is due to the short time horizon of the simulation ($T = 0.15$s). Within such a short time period, the the real rotor speeds lag behind the commands resulting in less control moment on the drone. Therefore, an accurate actuator model is essential for estimating the reachable set of a quadrotor.

The safe flight envelope with respect to flight with $V = 8$ m/s is given in Fig. 8 and Fig. 9. The safe envelope is defined as the intersection of the forward and backward reachable set. It can be seen from

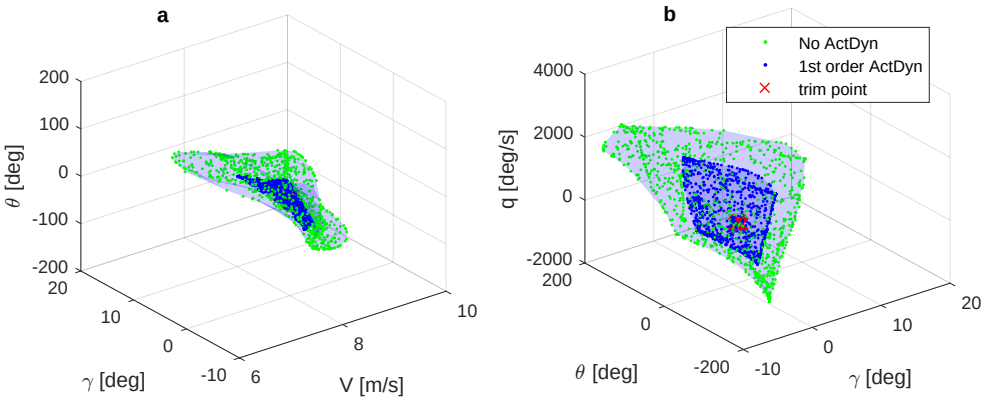

Figure 7: Forward reachable set comparison between simulations with and without actuator dynamics. a.) Forward reachable set projection on the $V-\gamma-\theta$ plane. b.) Forward reachable set projection on the $\gamma-\theta-q$ plane.

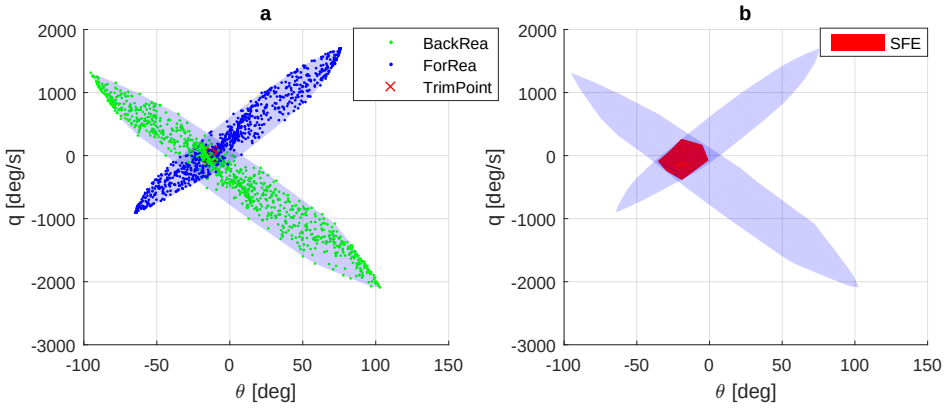

Figure 8: a.) Forward and backward reachable set projected in the $\theta-q$ plane. b.) The safe flight envelope is the intersection of the two reachable sets.

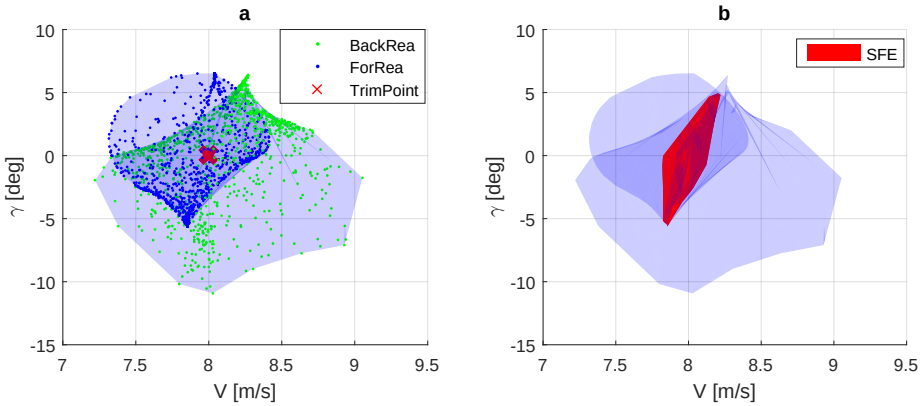

Figure 9: a.) Forward and backward reachable set projected in the $V-\gamma$ plane. b.) The safe flight envelope is the intersection of the two reachable sets.

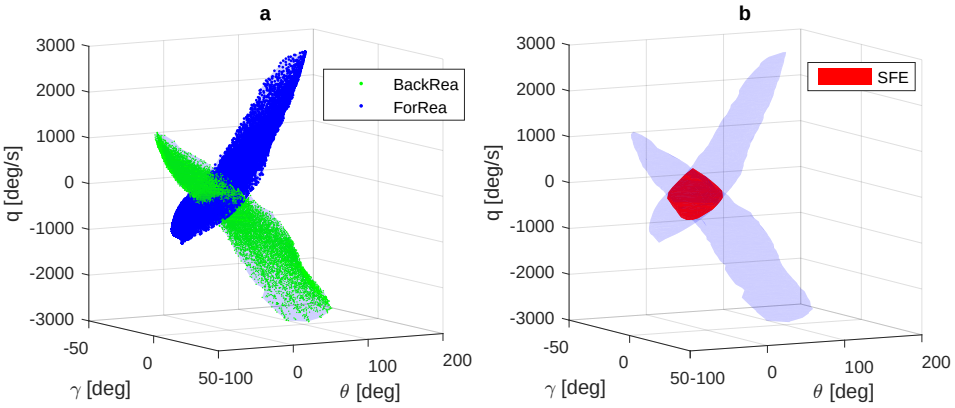

Figure 10: a.) Forward and backward reachable set from the trim curve, projected in $\theta - \gamma - q$ subspace. b.) The safe flight envelope.

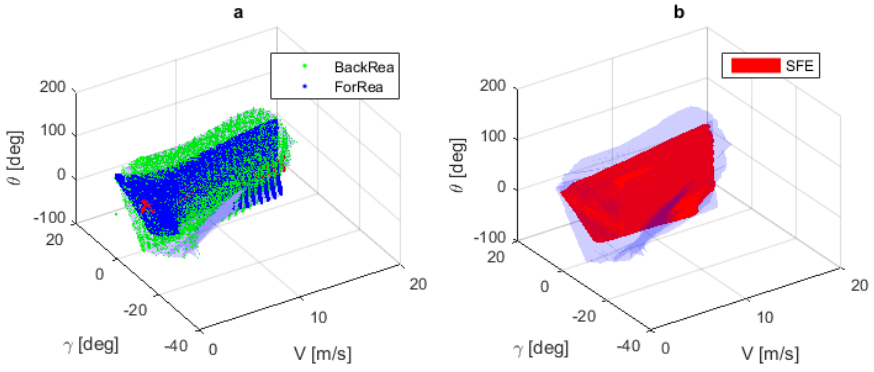

Figure 11: a.) Forward and backward reachable set from the trim curve, projected in $V - \gamma - \theta$ subspace. b.) The safe flight envelope.

the forward reachable set in Fig. 8, during the forward flight, a quadrotor can reach a pitch up rate over 1500 deg/s and a pitch angle up to 70 deg from the trim condition within 0.15 seconds. By contrast, the amount of pitch down angle and rate are smaller because of the pitch up aerodynamic moment in the forward flight. There is more information can be interpreted from the plot, for instance, the pitch angle from which the drone is recoverable within the time horizon and so forth.

In order to estimate the entire SFE with respect to a certain time horizon, the trim curve is then discretized into 20 points, from which 20 sets of Monte-Carlo simulations are conducted. The other parameters are the same as those presented above, that is, $p_c = 0.1$, $T = 0.15$ s, $N = 100$ and $N_{traj} = 1000$. The forward reachable set indicate the state space in which the drone is able to reach within 0.15 s from the trim curve. The backward reachable set indicate the state space from which the drone is possible to return the trim condition (which we define as safe) within $T = 0.15$ s. The intersection, i.e the safe flight envelope, indicate the state space in which and from which the drone is able to reach and return within $2T = 0.3$ s.

IV.B. Validation of the Reachable Sets

The forward and backward reachable sets have been validated in a 6-DoF simulation platform. For validating the forward reachable set, several trajectories originated from the trim curve have been generated with random rotor speed command. Fig. 12 shows the validation result in the subspace of V-γ-θ. The trajectories are confined to the forward reachable set within the time horizon, showing the validity of the forward reachable set.

As for the backward reachable set, the control input sequence archived in the envelope prediction procedure are retrieved for a trajectory originated from a randomly selected initial state closed to the boundary of the backward reachable set. Fig. 13 shows that all these trajectory are able to return the trim curve within the time horizon.

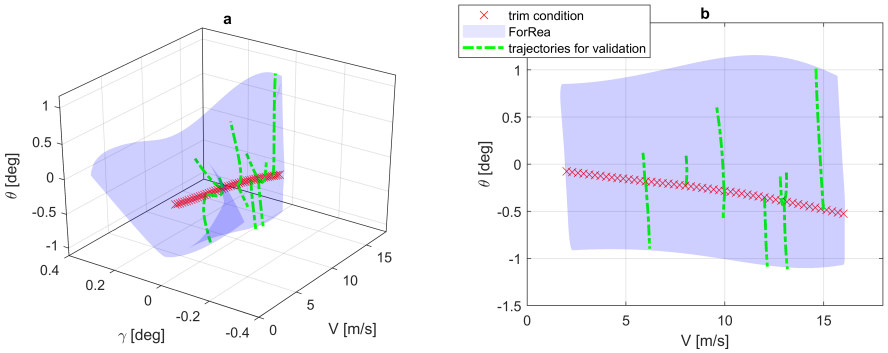

Figure 12: Validation of the forward reachable set with respect to the trim curve.

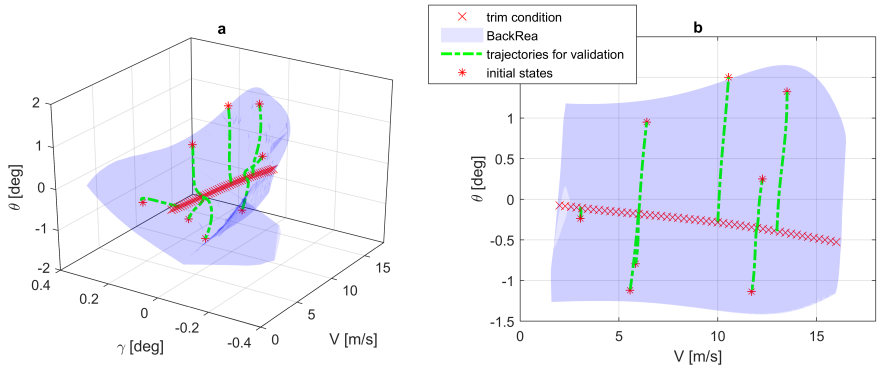

Figure 13: Validation of the backward reachable set with respect to the trim curve.

The validity of the reachable sets are found to be sensitive to the model uncertainties as is shown in Fig 14. If the aerodynamic model are identical to the one employed for estimating the backward reachable set, the drone is able to return to the trim condition (trajectories in dot-dash lines). However, if the aerodynamic

models are different from the one for estimating the reachable set, the trajectory may diverge as is shown in the solid lines. This is due to the fact that a quadrotor is open loop unstable and a slight difference in the aerodynamic model may lead to large divergence of the simulated trajectory, which hinders the selection of a large time horizon.

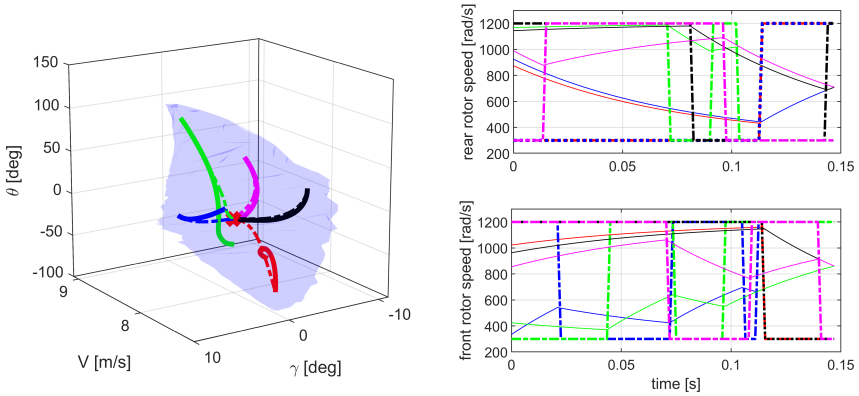

Figure 14: Validation of the backward reachable set with respect to the trim condition at $V = 8$m/s. a.) The trajectories from different initial conditions. The trajectories using precise aerodynamic models are in dot-dash line; the trajectories with different aerodynamic models are in solid line. b.) The corresponding control inputs of each trajectory. The command inputs are in dot-dash line; the real rotor speeds are presented by solid lines.

V. Conclusion

This report demonstrates a computationally efficient approach to estimate the reachable set of a nonlinear control-affine high-dimensional dynamic system. The method is utilized to estimate the longitudinal Safe Flight Envelope of a quadrotor. This application requires solving a 6 dimensional reachability problem in excess of the ability of the conventional Level Set approach. By contrast, the simulation based approach implemented in this research is able to estimate the 6-D reachable set efficiently. This provides an alternative approach of estimating the SFE for other types of aircraft.

References

[1]C. Belcastro and S. Jacobson, "Future Integrated Systems Concept for Preventing Aircraft Loss-of-Control Accidents," in *AIAA Guidance, Navigation, and Control Conference*, no. AIAA 2010-8142, (Reston, Virigina), pp. 1–17, American Institute of Aeronautics and Astronautics, 8 2010.

[2]C. M. Belcastro, R. L. Newman, J. Evans, D. H. Klyde, L. C. Barr, and E. Ancel, "Hazards Identification and Analysis for Unmanned Aircraft System Operations," *17th AIAA Aviation Technology, Integration, and Operations Conference*, no. June, 2017.

[3]J. Wilborn and J. Foster, "Defining Commercial Transport Loss-of-Control: A Quantitative Approach," *AIAA Atmospheric Flight Mechanics Conference and Exhibit*, no. August, pp. 1–11, 2004.

[4]N. Govindarajan, "An optimal control approach for estimating aircraft command margins," *Delft University of Technology*, 2012.

[5]J. Chongvisal, N. Tekles, E. Xargay, D. Talleur, A. Kirlik, and N. Hovakimyan, "Loss-of-Control Prediction and Prevention for NASA's Transport Class Model," *AIAA Guidance, Navigation, and Control Conference*, no. January, pp. 1–31, 2014.

[6]H. Pfifer, R. Venkataraman, and P. Seiler, "Quantifying Loss-of-Control Envelopes via Robust Tracking Analysis," *Journal of Guidance, Control, and Dynamics*, vol. 40, pp. 1042–1050, 4 2017.

[7]T. Lombaerts, S. Schuet, K. Wheeler, D. M. Acosta, and J. Kaneshige, "Safe Maneuvering Envelope Estimation based on a Physical Approach," in *AIAA Guidance, Navigation, and Control (GNC) Conference*, (Reston, Virginia), pp. 1–20, American Institute of Aeronautics and Astronautics, 8 2013.

[8]D. A. Thomas Lombaerts, Stefan Schuet and J. Kaneshige, "On-Line Safe Flight Envelope Determination for Impaired Aircraft," 2015.

[9]H. N. Nabi, T. Lombaerts, Y. Zhang, E. van Kampen, Q. P. Chu, and C. C. de Visser, "Effects of Structural Failure on the Safe Flight Envelope of Aircraft," *Journal of Guidance, Control, and Dynamics*, vol. 41, pp. 1257–1275, 6 2018.

[10]Y. Zhang, C. C. de Visser, and Q. P. Chu, "Database Building and Interpolation for a Safe Flight Envelope Prediction

System," in *2018 AIAA Information Systems-AIAA Infotech @ Aerospace*, no. January, (Reston, Virginia), pp. 1–13, American Institute of Aeronautics and Astronautics, 1 2018.

[11]S. Bansal, M. Chen, S. Herbert, and C. J. Tomlin, "Hamilton-Jacobi Reachability: A Brief Overview and Recent Advances," 2017.

[12]J. Maidens and M. Arcak, "Reachability Analysis of Nonlinear Systems Using Matrix Measures," *IEEE Transactions on Automatic Control*, vol. 60, no. 1, pp. 265–270, 2015.

[13]A. Girard and G. J. Pappas, "Verification Using Simulation," *Simulation*, pp. 272–286, 2006.

[14]A. Adimoolam, T. D. B, A. Donz, and J. Kapinski, "Safety Verification of Deep Neural Networks," vol. 1, no. May, pp. 483–503, 2017.

[15]H.-D. Tran, W. Xiang, N. Hamilton, and T. T. Johnson, "Simulation-Based Reachability Analysis for High-Index Large Linear Differential Algebraic Equations," 4 2018.

[16]J. Lygeros, "On reachability and minimum cost optimal control," *Automatica*, vol. 40, no. 6, pp. 917–927, 2004.

[17]S. Sun, R. J. Schilder, and C. C. D. Visser, "Identification of Quadrotor Aerodynamic Model from High Speed Flight Data," pp. 1–23.

[18]S. Sun, C. de Visser, and Q. Chu, "Quadrotor Gray-Box Model Identification from High-Speed," *Journal of Aircraft*, pp. 1–17, 2018.

[19]V. Klein and E. A. Morelli, *Aircraft System Identification: Theory and Practice*. Reston ,VA: American Institute of Aeronautics and Astronautics, 1 2006.

[20]G. M. Hoffmann, H. Huang, S. L. Waslander, and C. J. Tomlin, "Precision flight control for a multi-vehicle quadrotor helicopter testbed," *Control Engineering Practice*, 2011.